PAPER • OPEN ACCESS

Anthropogenic CO_2 emissions assessment of Nile Delta using XCO_2 and SIF data from OCO-2 satellite

View the article online for updates and enhancements.

Environmental Research Letters

PAPER

Anthropogenic CO_2 emissions assessment of Nile Delta using XCO_2 and SIF data from OCO-2 satellite

Ankit Shekhar[1,4,5] ⓘ, Jia Chen[1,5] ⓘ, Johannes C Paetzold[2], Florian Dietrich[1] ⓘ, Xinxu Zhao[1] ⓘ, Shrutilipi Bhattacharjee[1] ⓘ, Veronika Ruisinger[1] and Steven C Wofsy[3]

[1] Professorship of Environmental Sensing and Modeling, Technical University of Munich, Germany
[2] Chair of Computer Aided Medical Procedures & Augmented Reality, Technical University of Munich, Germany
[3] Department of Earth and Planetary Sciences and School of Engineering and Applied Sciences, Harvard University, Cambridge, Massachusetts, United States of America
[4] Department of Environmental Systems Science, ETH Zurich, Switzerland
[5] Authors to whom any correspondence should be addressed.

E-mail: ankit.shekhar@usys.ethz.ch and jia.chen@tum.de

Abstract

We estimate CO_2 emissions from the Nile Delta region of Egypt, using over five years of column-averaged CO_2 dry air mole fraction (XCO_2) data from the NASA's OCO-2 satellite. The Nile Delta has significant anthropogenic emissions of CO_2 from urban areas and irrigated farming. It is surrounded by the Sahara desert and the Mediterranean Sea, minimizing the confounding influence of CO_2 sources in surrounding areas. We compiled the observed spatial and temporal variations of XCO_2 in the Nile Delta region ($XCO_{2,del}$), and found that values for $XCO_{2,del}$ were on average 1.1 ppm higher than $XCO_{2,des}$ (mean XCO_2 in desert area). We modelled the expected enhancements of XCO_2 over the Nile Delta based on two global CO_2 emission inventories, EDGAR and ODIAC. Modelled XCO_2 enhancements were much lower, indicating underestimation of CO_2 emissions in the Nile Delta region by mean factors of 4.5 and 3.4 for EDGAR and ODIAC, respectively. Furthermore, we captured a seasonal pattern of XCO_2 enhancement (ΔXCO_2), with significantly lower ΔXCO_2 during the summer agriculture season in comparison to other seasons. Additionally, we used solar-induced fluorescence (SIF) measurement from OCO-2 to understand how the CO_2 emissions are related to agricultural activities. Finally, we estimated an average emission of CO_2 from the Nile Delta from 2014–2019 of 470 Mt CO_2/year, about 1% of global anthropogenic emissions, which is significantly more than estimated hitherto.

1. Introduction

Our planet Earth has witnessed about 40% increase in atmospheric CO_2 concentrations since the pre-industrial age. This increase is attributed to anthropogenic activities (IPCC 2013), primarily from combustion of fossil fuels. Agricultural activities are important sources of CO_2 associated with combustion of fossil fuels by farm machinery, biomass burning, and emissions from soil. Soil emissions can be especially high from intensively farmed, irrigated carbon rich soils in river deltas (Telmer and Veizer 1999, Hannam *et al* 2019).

Most global estimates of CO_2 emissions are provided by state-of-the-art emissions inventories which employ 'bottom-up' methods to quantify emissions, using human activity data and emission factors (Oda and Maksyutov 2011, Janssens–Maenhout *et al* 2019, Peylin *et al* 2013, Boden *et al* 2017, Oda *et al* 2018) as per the directions of IPCC (Intergovernmental Panel on Climate Change). These models have not been extensively tested for intensively farmed areas, like river deltas. Bottom-up methods use energy consumption data sets, such as fossil fuel consumption along with fuel purity, mix, efficiency, etc (see Boden *et al* 2017, Quéré *et al* 2018). There are discrepancies and uncertainties in the reported datasets on national scales (Miller *et al* 2013, Hutyra *et al* 2014, Liu *et al* 2015), especially for developing countries (Xue and Ren 2012). These discrepancies

can result in ∼40% to ∼100% uncertainty in emission estimations at the country and the local scales, respectively (Peylin *et al* 2013, Wang *et al* 2013).

Effective monitoring of greenhouse gas emissions is also essential to keep track of humanities long-term emission reduction goals for keeping the global warming below 2 °C compared to pre-industrial levels, as defined in the Paris agreement. Ground-based or airborne monitoring of these emissions can be a tedious and expensive task because of the spatial distribution of various anthropogenic emission sources (Mckain *et al* 2012, Chang *et al* 2014, Lindenmaier *et al* 2014, Chen *et al* 2016, 2020, Viatte *et al* 2017, Luther *et al* 2019). The most promising way to monitor these emissions with consistent precision at different spatial scales is the use of satellite-based measurements (Wang *et al* 2018).

Satellites like SCIAMACHY (Scanning Imaging Absorption Spectrometer for Atmospheric Cartography) and GOSAT (Greenhouse Gases Observing Satellite) have been previously used to detect and analyze anthropogenic CO_2 signatures (Yokota *et al* 2009, Kort *et al* 2012, Schneising *et al* 2013, Janardanan *et al* 2016). These studies generally suggested use of satellite-based observations with better spatial resolution to improve the detection of anthropogenic CO_2 emissions as the enhancement of CO_2 mixing ratio due to localized sources are a small fraction of the background values, thus making it a challenging task for low spatial resolution sensors to detect (Bovensmann *et al* 2010).

Here we use the observations from NASA's OCO-2 (Orbiting Carbon Observatory-2) satellite as a primary monitoring tool to assess the CO_2 emissions in the Nile Delta, one of the most important, intensively farmed regions in the world. The OCO-2 measures column-averaged dry air mole fraction of CO_2 (XCO_2) with high spatial resolution (∼3 km^2) (Crisp *et al* 2017) and precision (∼1 ppm). The megacity Cairo lies just to the south of the Delta. Both are surrounded by desert in three directions, except for the narrow Nile valley leading southward, with the Mediterranean in the north. OCO-2 tracks are situated over and nearby this area making it an excellent target for quantifying emissions using OCO-2 data. Our work builds on previous studies to detect localized emission sources (Yokota *et al* 2009, de Gouw *et al* 2014, Hakkarainen *et al* 2016, 2019, Kuze *et al* 2016, Nassar *et al* 2017, Schwandner *et al* 2017, Ye *et al* 2017, Wang *et al* 2018, Labzovskii *et al* 2019, Reuter *et al* 2019, Zheng *et al* 2019) using OCO-2 data.

We examine the spatiotemporal gradients of XCO_2 between the Nile Delta and surrounding desert over a 5 year period, and compared the observed enhancements to values modeled using global emission inventories. We find that the two investigated inventories underestimate CO_2 emission rates in the region by large factors with significant seasonality during the winter and summer agriculture season. We conclude that intensively-farmed deltaic areas may be significantly more important in global CO_2 emissions than appreciated hitherto.

2. Data and methods

2.1. Study area

The Nile Delta is considered to be one of the oldest cultivated areas in the world, having been continuously cultivated since 3000 B.C. (Negm *et al* 2017). It is a triangular shaped, tide-dominated delta (figure 1(a)) occupying about 2.5% of Egypt's area (∼25 000 km^2) and giving shelter to about 60% of its population (Zeydan 2005, Negm *et al* 2017). Moreover, 96% of Egypt's population is concentrated around Nile Delta (north of Cairo) along with Nile valley (south of Cairo) (Abd El-Kawy *et al* 2011). Since the construction of Aswan High Dam in 1970, the Nile Delta has received less input of nutrients and sediments from the river floods. This shift has resulted in intensive use of fertilizers for agriculture, thereby degrading the soil quality and potentially leading to loss of soil organic matter (Negm *et al* 2017). Furthermore, about 75 000 ha of fertile agricultural land was lost to urbanization within the Nile Delta between 1992 and 2015 (Radwan *et al* 2019). Nevertheless, the Nile Delta produces two-thirds of Egyptian crops (FAOSTAT 2019, www.fao.org/faostat/en/) with its still rich and fertile soil allowing two or more crops over the year (Osama *et al* 2017). Two main growing season in Nile Delta is the winter growing season (peak in January/February) and summer season (peak in July/August). Important winter crops are wheat, vegetable and clover crops, whereas in summer—maize, rice and cotton are extensively grown (El-Beheiry *et al* 2015). The Nile Delta today is mostly characterized by artificially irrigated agriculture and spreaded urban settlements (figure 1(a)), with minimal natural sources or sinks of CO_2.

2.2. OCO-2 satellite data

We used five years of XCO_2 data from NASA's OCO-2 satellite. The OCO-2 satellite was designed to accurately measure XCO_2 at kilometer-scale spatial resolution around 13:30 local time with a repeat cycle of 16 d (Crisp 2015) and 10 km swath (Bhattacharjee and Chen 2020). The satellite uses the Atmospheric CO_2 Observations from Space (ACOS) algorithm (Wunch *et al* 2011a, 2011b, Crisp *et al* 2012, O'Dell *et al* 2012). We used the high quality measurement soundings of the latest version of the OCO-2 Level 2 Version 9 Lite product from September 2014 to July 2019 provided by the NASA's Jet Propulsion Laboratory website (https://co2.jpl.nasa.gov/build/?dataset=OCO2L2Std v8&product=FULL#download). The measurement soundings are obtained using an improved bias-correction approach and are pre- and post-filtered for potentially unreliably measurements (O'Dell *et al* 2018). The downloaded measurement data
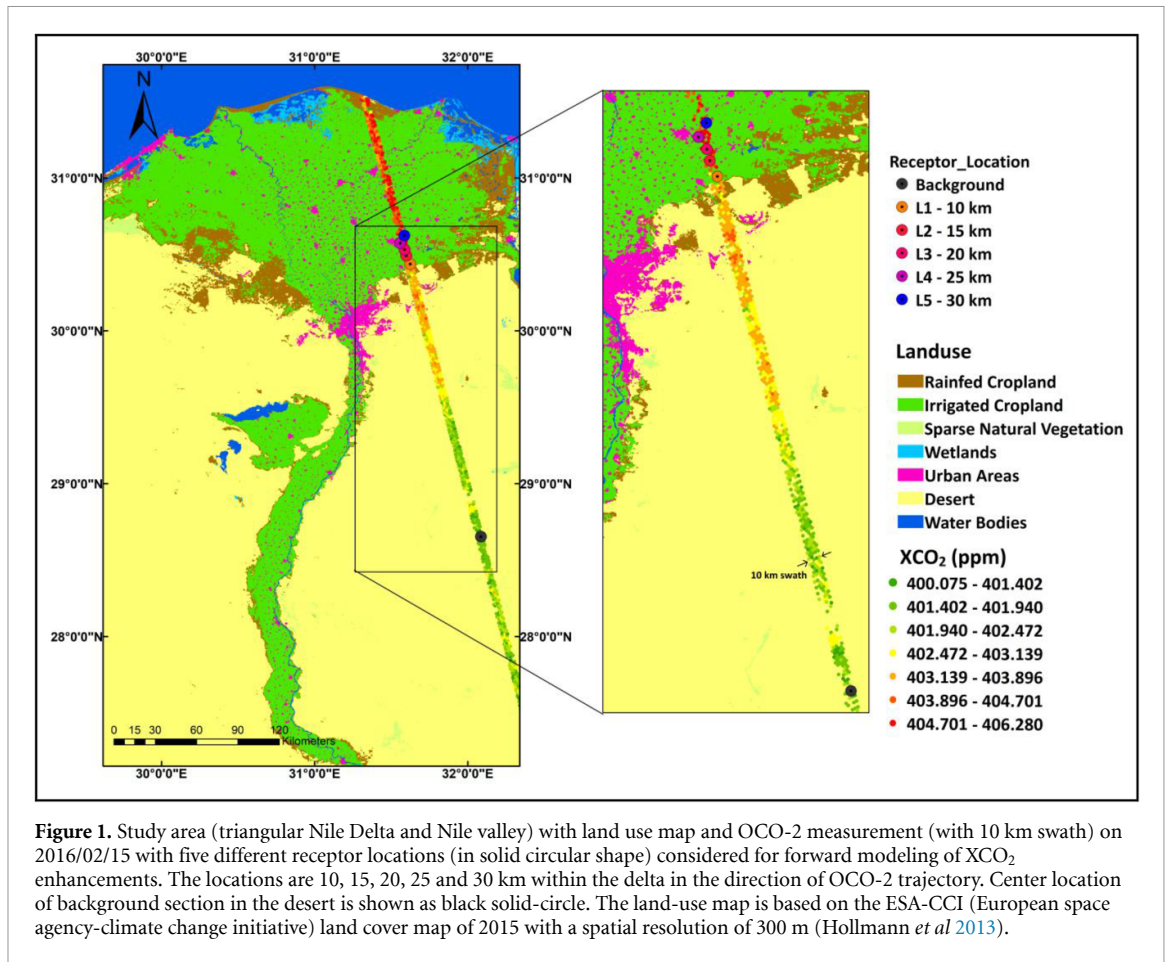
Figure 1. Study area (triangular Nile Delta and Nile valley) with land use map and OCO-2 measurement (with 10 km swath) on 2016/02/15 with five different receptor locations (in solid circular shape) considered for forward modeling of XCO_2 enhancements. The locations are 10, 15, 20, 25 and 30 km within the delta in the direction of OCO-2 trajectory. Center location of background section in the desert is shown as black solid-circle. The land-use map is based on the ESA-CCI (European space agency-climate change initiative) land cover map of 2015 with a spatial resolution of 300 m (Hollmann *et al* 2013).

also contain surface wind velocity information at each measurement sounding taken from the NASA's GEOS5-FP-IT (Goddard Earth Observing System Version 5-Forward Processing for Instrument Teams). Each trajectory of OCO-2 measurement covers both the delta and desert area (figure S1 (available online at stacks.iop.org/ERL/15/095010/mmedia)), which enables us to quantify the spatial (delta-desert) XCO_2 gradient.

In addition to XCO_2 data, we also employed OCO-2's SIF (Solar-induced fluorescence) data. SIF is a signal emitted from plants/crops during photosynthesis, thus indicating photosynthetic activities (Sun *et al* 2017, Shekhar *et al* 2019, Castro *et al* 2020). OCO-2 measures SIF at two wavelengths, 757 nm and 771 nm (Frankenberg *et al* 2014, 2015), based on the infilling of the Fraunhofer lines (Frankenberg *et al* 2011). We used SIF (measured at 757 nm) to help understand how the CO_2 emissions from the Nile Delta were related to agricultural activities.

2.3. Emission inventories

We computed the expected values of XCO_2 over the Delta, compared to surrounding desert areas, using two CO_2 emission inventories, EDGAR (Emissions Database for Global Atmospheric Research) and ODIAC (Open-source Data Inventory for Anthropogenic CO_2). Both are constructed based on the

IPCC methodology. The latest version of EDGAR v5.0 (Crippa *et al* 2020) was recently made available. It provides global annual CO_2 emissions at $0.1° \times 0.1°$ spatial resolution until 2018. EDGAR emissions are calculated using a bottom-up methodology: the inventory scales activity data, which is based on international annual statistics with the best-available emission factors. Then, it uses the monthly share and spatial proxies such as population and road density to downscale the national or state-level data to a finer spatial resolution. We used the CO2_excl_short-cycle_org_C variable of the EDGAR v5.0 which includes total CO_2 emissions (in $kgCO_2$ $(m^2 \ s)^{-1}$) from the considered fossil fuel sources such as fossil fuel combustion, various non-metallic mineral processes like cement production, various metallic and chemical production processes, urea productions and agricultural liming processes. The EDGAR v5.0 dataset was downloaded from the European Commission's Joint Research Centre-EDGAR website (https://edgar.jrc.ec.europa.eu/overview.php?v=50_GHG). Mean EDGAR emissions over the Nile Delta from 2014–2018 was 108 Mt CO_2/year.

The latest ODIAC v2019 provides monthly CO_2 emissions (in tons of Carbon/(km^2-month)) from fossil fuel combustions at a much higher spatial resolution of 1 km $\times$ 1 km (GeoTIFF file format) till the end of 2018 (Oda *et al* 2018).

A hybrid approach is implemented to construct the ODIAC emission inventory, which integrates national emission estimates produced by CDIAC (Carbon Dioxide Information Analysis Center, Andres *et al* 1996) and nightlight data with individual power plant emissions/location profiles (Oda and Maksyutov 2011). The ODIAC v2019 dataset was downloaded from the CGER-NIES (Center for Global Environmental Research, National Institute for Environmental Studies) website (http://db.cger.nies.go.jp/dataset/ODIAC/DL_odiac2019.html).

Since neither the EDGAR nor the ODIAC dataset was fully available for the time period of this study (September 2014–July 2019), we used the latest available data point for each inventory for the remaining time period, i.e. the EDGAR and ODIAC estimates of 2018 were used for the year of 2019. It is important to note that neither of these two emission inventories include CO_2 emission from agricultural soil degradation. Both EDGAR and ODIAC emission datasets are widely used by the international carbon cycle research community (Quéré *et al* 2018). Mean ODIAC emissions over the Nile Delta from September 2014–July 2019 was 136.5 Mt CO_2/year. Figure S3 shows the CO_2 emission map for Nile Delta as per EDGAR and ODIAC.

2.4. Modelling methods

To simulate the enhancement of XCO_2 values from the local CO_2 emissions sources we employed a forward model based on the emission inventories and an atmospheric transport model.

For any location, the XCO_2 can be modelled as the sum of the initial background concentration and the enhancement due to the upstream sources and sinks (Gerbig *et al* 2003, Hu *et al* 2018a). Equations (1) and (2) describe our calculations:

$$XCO_{2.fm} = XCO_{2.bkg} + XCO_{2.enh} \qquad (1)$$

$$XCO_{2,enh} = \sum_{i=1}^{N_x} \sum_{j=1}^{N_y} \left[footprint\left(x_i, y_j\right) \right.$$
$$\left. \times emission\left(x_i, y_j\right) \right] \qquad (2)$$

where, $XCO_{2,fm}$ is the forward modelled concentration for any location, $XCO_{2,bkg}$ is an initial background XCO_2 value and $XCO_{2,enh}$ is the enhancement due to upstream CO_2 emission sources. The 'footprint' is obtained from an atmospheric transport model and the 'emission' data are obtained from the emission inventories (more information below). Therefore, $XCO_{2,enh}$ is the summation of the enhancements caused by all locations (x_i, y_j): $i = 1,2…N_x$; $j = 1,2…N_y$, in the study domain containing the Nile Delta and valley (Latitude:[26, 32]; Longitude:[29, 33]). For the case of simplicity here, we have neglected the effect of sinks on $XCO_{2,enh}$ as the Nile Delta
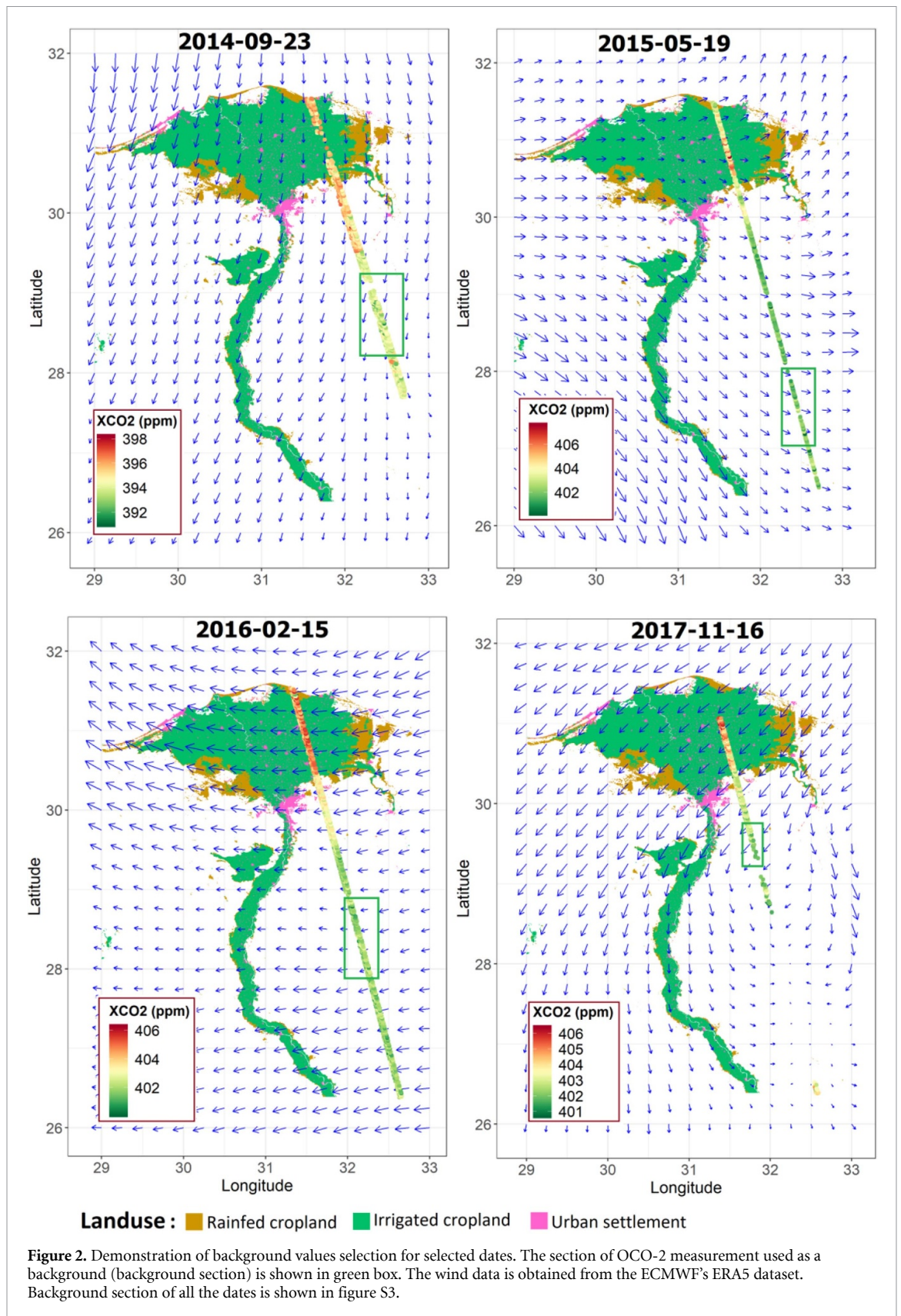
is characterized by minimal or no natural vegetation, and net emissions are plainly positive. To study the XCO_2 enhancement in the Nile Delta we applied a local regression smoothing (LOESS, Jacoby 2000) with loess parameter (span) of 0.15 to the XCO_2 concentrations along the OCO-2 trajectory (latitude-wise) for each measurement day, and these locally regressed XCO_2 ($XCO_{2,O}$) values were used for further calculation.

Since OCO-2 measures XCO_2 along a narrow swath of 10 km (figure 1), selection of background concentration ($XCO_{2,bkg}$) can be tedious. In this study, we leveraged the wind data from ECMWF's ERA5 dataset (Copernicus Climate Change Service (C3S) 2017) to select a particular section of one degree latitude range (background section) of XCO_2 values in the desert that did not pass over the Nile Delta as $XCO_{2,bkg}$. The selection of 'background section' was semi-automated for all the 32 dates. The semi-automated process involved visual inspection and automated selection of the background section. The detailed procedure is given in supplementary section S1. Figure 2 illustrates the background section for few dates. For example on 2014-09-23, the wind direction is north, contaminating the proximate observations with CO_2 from the Delta, so we selected the lower section of OCO-2 measurements (shown in green box in figure 2), where the wind was coming from the east side. Similarly, for 2015-05-19, the selected section does not have any influence from Nile Delta and minimal influence from the Nile valley. The mean of the locally smoothed XCO_2 values within this section was taken as a $XCO_{2,bkg}$ for each day. The selected background section for all the other dates is shown in figure S3.

Calculation of $XCO_{2,enh}$ requires footprint information from the atmospheric transport model, and local emission data. The geographic distributions of emissions were adopted from EDGAR and ODIAC (section 2.2). Here, we simulated the footprints using the STILT (Stochastic Time-Inverted Lagrangian Transport) model that is based on HYSPLIT model (Lin *et al* 2003, Fasoli *et al* 2018, Wu *et al* 2018). The STILT model simulates convective and diffusive air transport patterns by releasing a certain amount of particles (N) from a receptor (i.e. an observation location in this case) and tracking the particles backwards in time (Hu *et al* 2018b). Thus, the STILT footprints are equivalent to the sensitivity of XCO_2 (unit of ppm·m²·s·μmol^{-1}) at the receptor location with respect to changes in surface flux (Gerbig *et al* 2003).
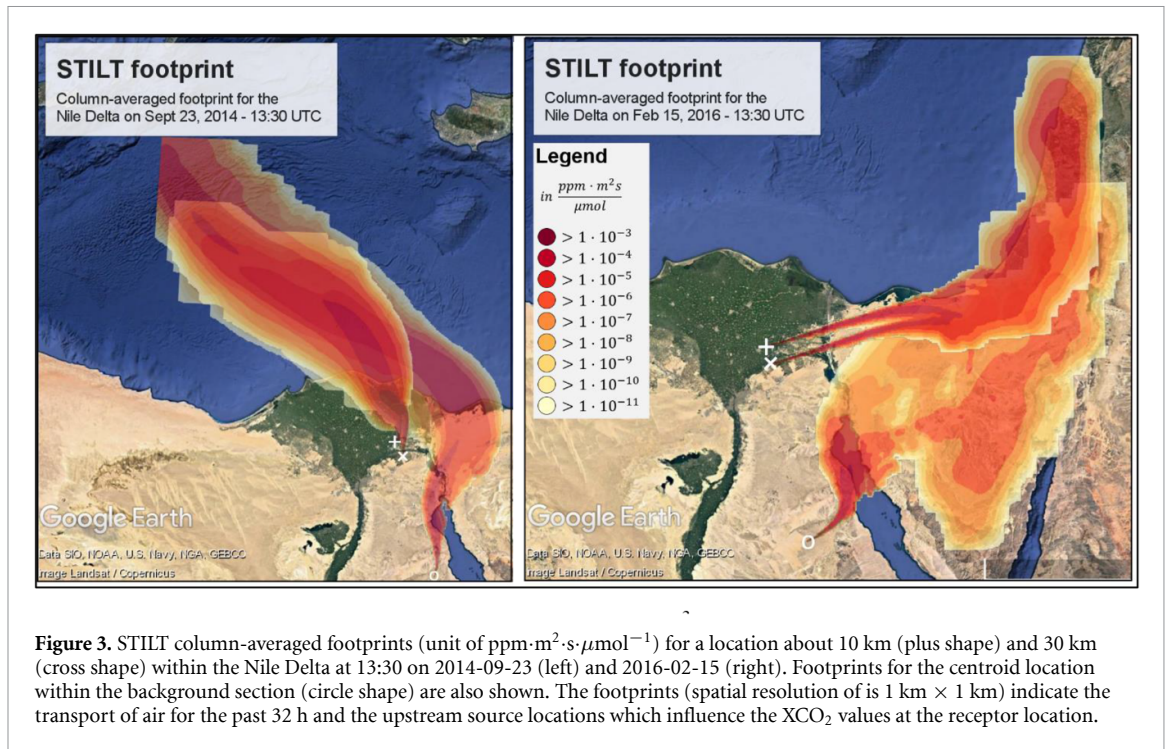
Our STILT simulation was based on ERA5 meteorological data and we chose a backward time of 32 h and N = 500 particles and 11 vertical levels for each receptor location. Figure 3 shows column averaged STILT footprints for 2014-09-23 and 2016-02-15 at 13:30 (local overpass time of OCO-2). Finally for each OCO-2 trajectory we chose 5 receptor locations

Figure 2. Demonstration of background values selection for selected dates. The section of OCO-2 measurement used as a background (background section) is shown in green box. The wind data is obtained from the ECMWF's ERA5 dataset. Background section of all the dates is shown in figure S3.

within the Nile Delta at a distance of 10, 15, 20, 25 and 30 km along the OCO-2 trajectory to calculate $XCO_{2,fm}$ (in ppm), which is the accumulated CO_2 enhancement occurring over the 32 h back trajectory at the receptor location due to emissions from the upstream sources. Figure 1 shows the receptor locations along the delta and within the background section for OCO-2 measurements on 2016-02-15. It is also evident from figure 3 that the footprints of the background receptor are not influenced by the Nile

Figure 3. STILT column-averaged footprints (unit of ppm·m^2·s·μmol^{-1}) for a location about 10 km (plus shape) and 30 km (cross shape) within the Nile Delta at 13:30 on 2014-09-23 (left) and 2016-02-15 (right). Footprints for the centroid location within the background section (circle shape) are also shown. The footprints (spatial resolution of is 1 km × 1 km) indicate the transport of air for the past 32 h and the upstream source locations which influence the XCO$_2$ values at the receptor location.

Delta area. Ultimately we compared the XCO$_{2,\text{fm}}$ with the LOESS smoothed OCO-2's XCO$_2$ value at the receptor locations (XCO$_{2,\text{O}}$) for each OCO-2 trajectory over study period (2014–2019) to estimate CO$_2$ emissions based on the two inventory data.

3. Results and discussions

3.1. Spatiotemporal variation of XCO$_2$ and SIF

We studied 62 d of OCO-2 measurements over the Nile Delta and desert area spanning five years of observations. We observed the expected steady seasonal cycle in XCO$_2$ concentration over the delta (XCO$_{2,\text{del}}$) and the desert (XCO$_{2,\text{des}}$) from 2014 to 2019 (figure 4). About 80% of the measurements showed a mean XCO$_{2,\text{del}}$ of 1.11 (0.83,1.21) (95% confidence interval) ppm higher than mean XCO$_{2,\text{des}}$ with a maximum ΔXCO$_2$ (XCO$_{2,\text{del}}$—XCO$_{2,\text{des}}$), of 2.2 ppm. Expectedly, consistent higher SIF values in the Nile Delta indicated the agricultural production (figure S4), with high SIF values during the months of peak of winter growing season (DJF) and summer growing season (JJA), but the latter season showed significantly lower ΔXCO$_2$ values (figure 5). This seasonal pattern of ΔXCO$_2$ can be attributed to the river flow dynamics and crops grown in the winter and summer season. The delta receives sediment and carbon-rich water during the winter season from the Aswan high dam (El Gamal and Zaki 2017), which is recycled and also used in the summer season. The emissions from newly arrived carbon-rich soil (carbon source) could result in high ΔXCO$_2$. However in summer, high photosynthetic activity of well-irrigated maize and rice during the mid-day could be

a significant carbon sink (Rana *et al* 2016, She *et al* 2017) with reduced CO$_2$ emission from soil, thereby resulting in lower XCO$_2$ values in the delta. A detailed study combined with cropping pattern and river flow dynamics could give insight that is more accurate. On average higher SIF values correlated with higher XCO$_2$, which might not be expected for forest, but because of all the fossil fuel and soil CO$_2$ emissions associated with the farming and irrigation in the Nile Delta (figure 5 and S5).

The OCO-2 clearly captured the latitudinal variation of XCO$_2$ concentrations along its trajectory as depicted in figure 6. Transportation of CO$_2$ plumes from emission sources in the delta region including Cairo city and Nile valley by the wind resulted in comparatively high XCO$_2$ values in the downwind desert area. For example, on 2015-05-19 the CO$_2$ emissions from Cairo results in as much as 3 ppm higher XCO$_2$ values in the downwind desert area compared to the southern desert, with minimum influence from the Nile Delta or valley (figure 6). Furthermore, emissions from the Nile valley clearly resulted in elevated XCO$_2$ values in the downwind desert area, for example on 2018-11-03 (figure 6, latitude: ~26.5 deg.). Such wind transport of CO$_2$ plume resulted in high XCO$_2$ values in the desert region. Thus, OCO-2's XCO$_2$ measurement clearly demonstrates the capability to measure local enhancement in XCO$_2$ values.

3.2. Forward modeling of emission inventories

Out of the 62 d of OCO-2 measurements, many days had sparse measurements over the Nile Delta and desert area, making it difficult to select background XCO$_2$ values. Therefore, before performing the forward modeling of emission inventories to calculate
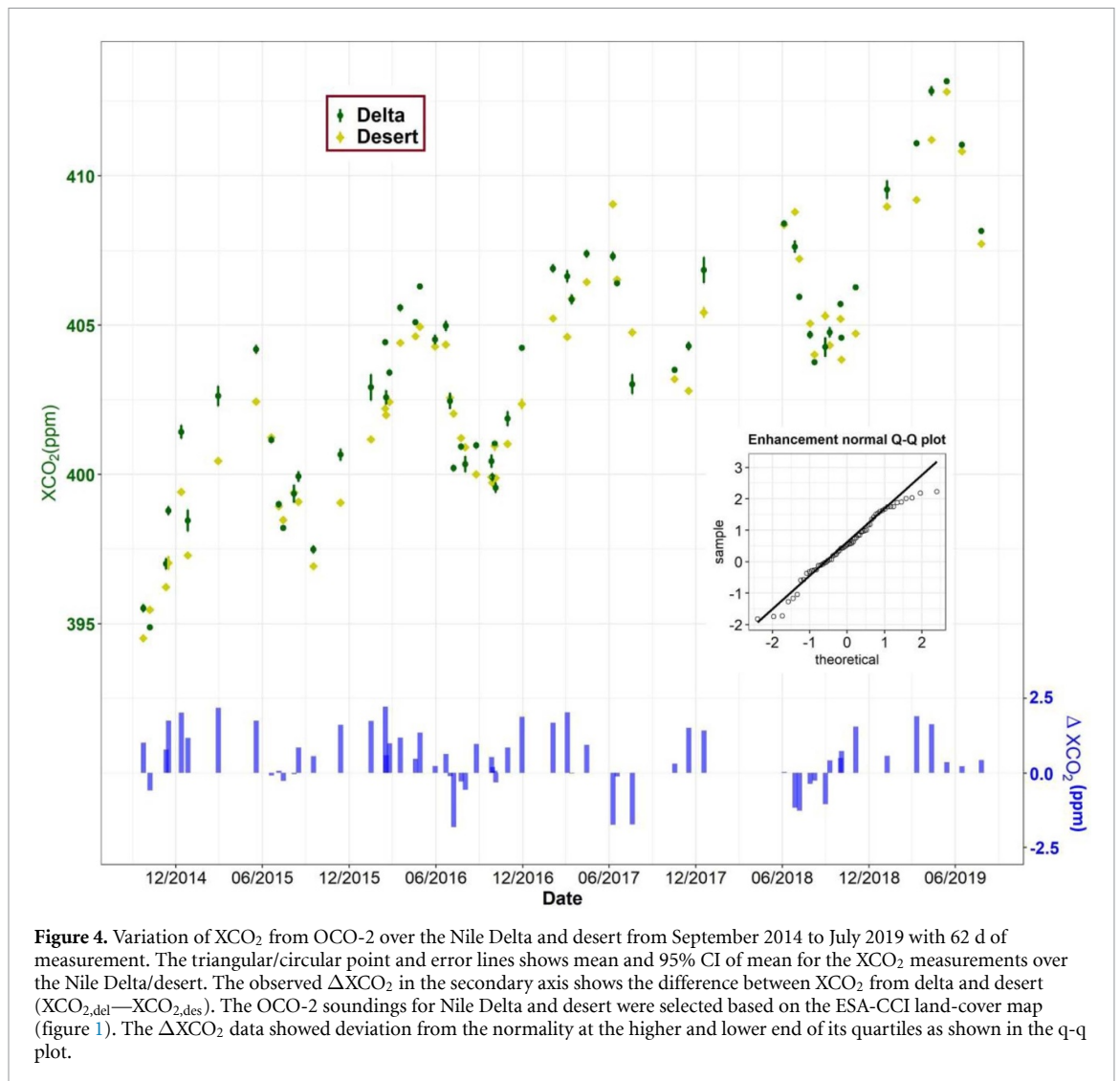
Figure 4. Variation of XCO_2 from OCO-2 over the Nile Delta and desert from September 2014 to July 2019 with 62 d of measurement. The triangular/circular point and error lines shows mean and 95% CI of mean for the XCO_2 measurements over the Nile Delta/desert. The observed ΔXCO_2 in the secondary axis shows the difference between XCO_2 from delta and desert ($XCO_{2,del}$—$XCO_{2,des}$). The OCO-2 soundings for Nile Delta and desert were selected based on the ESA-CCI land-cover map (figure 1). The ΔXCO_2 data showed deviation from the normality at the higher and lower end of its quartiles as shown in the q-q plot.
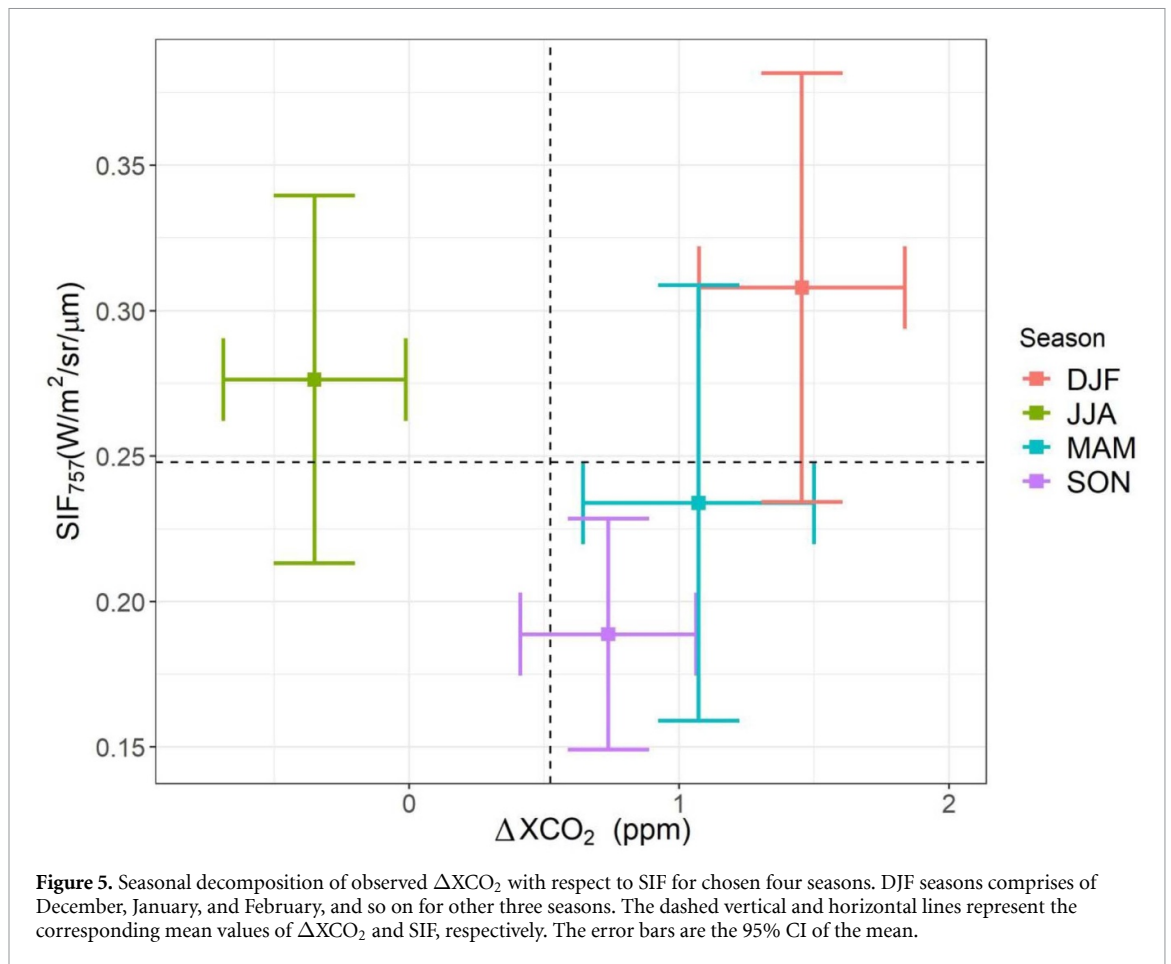
$XCO_{2,m}$, we applied a threshold criteria of minimum 100 and 200 measurements over the Nile Delta and desert area, respectively. Finally, 32 d satisfied the above criteria. Correspondingly, we performed forward modeling calculations on 5 locations at 32 different dates from 2014 to 2019. Two out of 32 d (2017-06-09 and 2018-07-07) showed consistently higher measurement values in the desert area resulting in higher $XCO_{2,bkg}$ values compared to the $XCO_{2,O}$ values at the receptor locations. These two dates occur during the peak of summer growing season and might indicate the agricultural crops grown (e.g. maize) in summer as a CO_2 sink.

For all 32 dates at 5 locations (total 160 receptor locations), the observed enhancements ($XCO_{2,O}$—$XCO_{2,bkg}$) averaged 1.21 (1.05,1.36) ppm. The calculated enhancements were much lower, 0.27 (0.23,0.32) ppm and 0.36 (0.31,0.43) ppm based on EDGAR and ODIAC, respectively (figure 7). Very prominent enhancements of as high as 1.7 ppm and 4 ppm by EDGAR and ODIAC, respectively were obtained for receptor location in the Cairo city (figure 7).

Over the 32 d of study, 23 d showed underestimation of modelled enhancement (figure 8), which indicates high underestimation of CO_2 emission by the emission inventories. Our calculations indicate an underestimation by a mean emission factor (MEF) (95% confidence interval) of 4.53 (4.34, 4.68) and 3.36 (3.19, 3.45) (calculated as a ratio of the mean observed enhancement over all the days, divided by the mean modelled enhancement for all days, and bootstrapped) for EDGAR and ODIAC, respectively. Based on these calculated MEFs we also estimated the CO_2 emissions from the Nile Delta based on scaling up the two emission inventories. Our estimates of mean CO_2 emission are about 489 Mt CO_2/year and 457 Mt CO_2/year based on EDGAR and ODIAC inventory over the study period (September 2014–July 2019).

Our estimate compares relatively well with recent CO_2 emissions of about 1500 Mt CO_2/year estimated from Yangtze River Delta in 2013 based on remote sensing (nighttime light) and statistical data (socioeconomic indicators) by Zhou *et al* (2019) as shown in table 1. The Yangtze River Delta is

Figure 5. Seasonal decomposition of observed ΔXCO_2 with respect to SIF for chosen four seasons. DJF seasons comprises of December, January, and February, and so on for other three seasons. The dashed vertical and horizontal lines represent the corresponding mean values of ΔXCO_2 and SIF, respectively. The error bars are the 95% CI of the mean.

about 4 times larger than Nile Delta and is similarly characterized by intense urbanization and agricultural activity. However, our emissions estimates are quite high as compared to values obtained for the Pearl River Delta (table 1). Xu *et al* (2018) used urbanization indicators (like land, population and economic urbanization) to estimate carbon emissions in Pearl River Delta and also highlighted uncertainties in emission estimates due to selection of indicators (Peng *et al* 2017). None of the above studies included emissions from exploited/degrading carbon-rich agriculture soils, which may be a significant source in Nile Delta.

Uncertainties in CO_2 emission inventories have been reported for developing countries, e.g. India and China (Guan *et al* 2012, Xue and Ren 2012, Janardanan *et al* 2016), and have mostly been attributed to uncertainties in the national level energy statistics and human activity data used to construct inventory data sets. Furthermore, the plot of ΔXCO_2 and SIF (indication of agriculture activity) in figures 5 and S5, clearly shows seasonal differences, especially for the two main growing season (winter and summer) with lower XCO_2 for the Delta during the summer growing season. We also calculated the seasonal MEFs for each season and found that the factors for the JJA season (MEF $\sim$ 1.05) was significantly lower than MAM season (MEF $\sim$ 5–8), and SON season

(MEF $\sim$ 6–11) (see table S1). However, for DJF season, only two OCO-2 measurements dates have sufficient observations over the Nile Delta and desert area for the emission assessments (2015-02-15 and 2017-02-03). There are very high differences between modelled and observed XCO_2 enhancements (>2 ppm in figure 8), which resulted in very high MEF ($\sim$30 to 50, see table S1), which may be biased due to less measurement samples. Nevertheless, such strong signal of seasonal variation of XCO_2 can be attributed directly or indirectly to agricultural farming and irrigation activities associated with the sediment-rich river inflow that occurs during the winter season.

Direct agriculture emissions include tillage enhanced soil respiration and crop residue burning, whereas indirect emission comes from fossil fuel consumption by farm machineries for various intercultural activities like tilling, weeding, harvesting etc, and pumps for irrigation. In 2010, as per report from EAS (2014), irrigation pumps (mostly diesel pumps) were used in 75% of the cultivated area. El-Gafy and El-Bably (2016) measured an average emission of 6.55 tCO_2/ha from on-farm diesel pumps used for irritation.

Apart from agricultural activities, anthropogenic emissions from transportation, industrial and household use (combined energy statistics) of various distributed cities in the Nile Delta might also
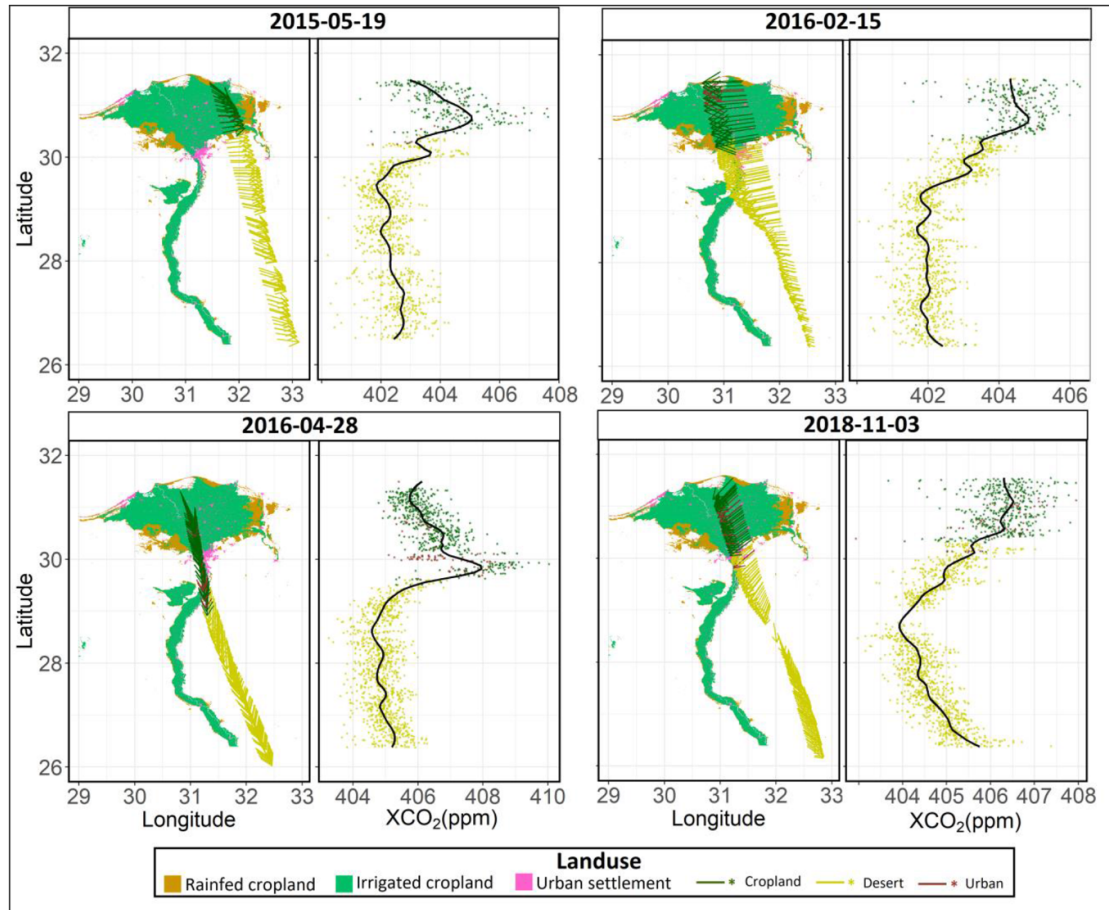
Figure 6. Latitudinal variation of XCO_2 in the Nile Delta and desert and wind direction at 13:30 for a few selected dates. Black solid line is the local regression (loess) smoothed result with span = 0.15. The urban settlement in the lower end of the delta area is the Cairo megacity. The arrows represent the wind direction at the OCO-2 measurement points.
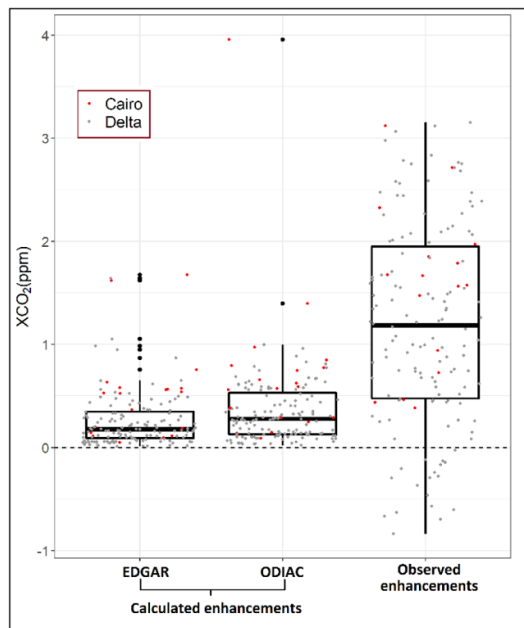

Figure 7. Comparison of modelled/calculated XCO_2 enhancements ($XCO_{2,enh}$) using the EDGAR and the ODIAC emission inventories with the observed enhancements ($XCO_{2,O}$—$XCO_{2,bkg}$) for receptor locations. Red dots represents receptor location in Cairo megacity, whereas grey dots are for receptor locations at Nile Delta excluding Cairo megacity. The horizontal line inside the box plots represent the median value.

Table 1. Comparison of CO_2 emissions from Nile Delta with other river delta.

	Nile Delta	Pearl River Delta	Yangtze River Delta
Country	Egypt	China	China
Area (km^2)	~25 000	~40 000	~110 000
Population (millions)	39	56	96
Year	2014–2019	2014	2013
Data	OCO-2 XCO2	Urbanization indicators	City Panel remote sensing and statistical data
Emission estimate (Mt CO_2/year)	473[a]	151	1450
Reference	Present study	Xu *et al* (2018)	Zhou *et al* (2019)

[a] Average of CO_2 emission based on EDGAR and ODIAC data
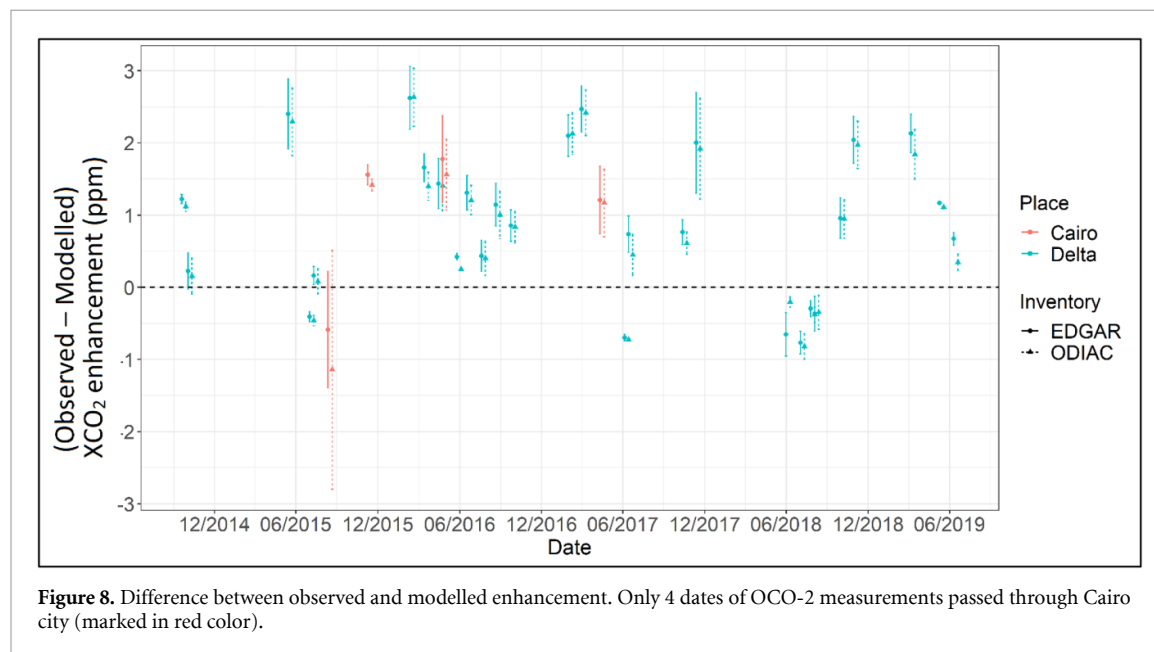
Figure 8. Difference between observed and modelled enhancement. Only 4 dates of OCO-2 measurements passed through Cairo city (marked in red color).

be under-reported in these global emission inventories (Guan *et al* 2012). Gately and Hutyra (2017) argued that global emission inventories (like ODIAC) appear to deflect from spatial patterns in source activity in comparison to national scale inventories, and thus the former might not accurately represent anthropogenic emissions at subnational or urban scales. Our calculated delta emissions are based on yearly (for EDGAR) and monthly (ODIAC) average of CO_2 emissions, whereas the OCO-2 XCO$_2$ measurements are instantaneous, at 13:30 local time. This can result in under-/over-estimation of calculated enhancements as CO_2 emissions vary diurnally, weekly and seasonally, especially for urban areas. Burri *et al* (2009) measured CO_2 fluxes using the eddy covariance method at the University of Cairo and showed that the CO_2 fluxes have a significant diurnal and weekly variation, with peak CO_2 flux occurring between 14:00 and 16:00 and minimum flux on Friday (rest day due to Muslim prayer day on Friday). In our study, ODIAC performed a little better compared to EDGAR, as the former gives monthly average estimates and thus has the capability to capture the seasonal variability of CO_2 emissions, which cannot be implied for the latter.

4. Conclusions

Our study assesses CO_2 emissions from the Nile Delta, which is particularly characterized by anthropogenic activities such as agriculture and urbanization, using the OCO-2 satellite observations of atmospheric CO_2 concentrations. We found that emission inventory-based modelled XCO$_2$ values were significantly lower than the satellite-based observed XCO$_2$ values in the Nile Delta (factor 4.53 [4.34, 4.68] for EDGAR and 3.36 [3.19, 3.45] for ODIAC), indicating underestimation of CO_2 emissions reported in the emission inventory. We combined XCO$_2$ data with SIF to relate CO_2 emissions from agricultural production in the Nile Delta. Our emission estimate for the Nile Delta was about 1% of the global anthropogenic CO_2 emission and was comparable to the scaled CO_2 emissions estimated for the Yangtze River Delta considering the differences in size. Our results are particularly important in the context of uncertainties in national level reported energy/activity statistics for developing nations, which results in underestimation of their CO_2 emissions by the state-of-the art emission inventories. Our study provides an approach for verification of bottom-up emission inventories

using satellite-based XCO_2 measurement over consistently emitting local and regional sources. The latest OCO satellite, OCO-3 (launched in May 2019 and data available since January 2020), which also measures XCO_2 and SIF, captures data of larger area ($100\,km \times 100\,km$) in a snapshot mode with the same high spatial resolution, thus providing the opportunity to assess spatial variability of carbon emissions of larger area based on our approach. Based on the findings of our study, we recommend eddy covariance flux measurements in such a carbon-rich delta to quantify the seasonality of CO_2 emissions, which could be used to improve the emission inventories. Finally, we call for more research in estimating possible uncertainties and thereby improve the accuracy of the emission inventories especially for countries with intense agriculture activities.

Acknowledgments

Data availability statement

The data that support the findings of this study are openly available at the OCO-2 data portal at https://co2.jpl.nasa.gov/#mission=OCO-2

ORCID iDs

Ankit Shekhar ⬤ https://orcid.org/0000-0003-0802-2821
Jia Chen ⬤ https://orcid.org/0000-0002-6350-6610
Florian Dietrich ⬤ https://orcid.org/0000-0002-3069-9946
Xinxu Zhao ⬤ https://orcid.org/0000-0002-2251-3451
Shrutilipi Bhattacharjee ⬤ https://orcid.org/0000-0002-6288-0942

References

Abd El-Kawy O R, Rød J K, Ismail H A and Suliman A S 2011 Land use and land cover change detection in the western Nile Delta of Egypt using remote sensing data *Appl. Geogr.* **31** 483–94

Andres R J, Marland G, Fung I and Matthews E 1996 A 1° × 1° distribution of carbon dioxide emissions from fossil fuel consumption and cement manufacture, 1950–1990 *Global Biogeochem. Cycles* **10** 419–29

Bhattacharjee S and Chen J 2020 Prediction of satellite-based column CO_2 concentration by combining emission inventory and LULC information *IEEE Trans. Geosci. Remote Sens.* 1–16

Boden T A, Marland G and Andres R J 2017 Global, regional, and national fossil-fuel CO_2 emissions, Carbon Dioxide Information Analysis Center, Oak Ridge National Laboratory, US Department of Energy (https://doi.org/10.3334/CDIAC/00001_V2017)

Bovensmann H, Buchwitz M, Burrows J P, Reuter M, Krings T, Gerilowski K, Schneising O, Heymann J, Tretner A and Erzinger J 2010 A remote sensing technique for global monitoring of power plant CO_2 emissions from space and related applications *Atmos. Meas. Tech.* **3** 781–811

Burri S, Frey C, Parlow E and Vogt R 2009 CO_2 fluxes and concentrations over an urban surface in Cairo/Egypt. *Paper Presented at the Seventh Int. Conf. on Urban Climate Organized by the IAUC, Yokohama, 29 June–3 July*

Castro A O, Chen J, Zang C S, Shekhar A, Jimenez J C, Bhattacharjee S, Kindu M, Morales V H and Rammig A 2020 OCO-2 solar-induced chlorophyll fluorescence variability across ecoregions of the Amazon basin and the extreme drought effects of El Niño (2015–2016) *Remote Sens.* **12** 1202

Chang R Y W *et al* 2014 Methane emissions from Alaska in 2012 from CARVE airborne observations *Proc. Natl Acad. Sci.* **111** 16694–9

Chen J, Dietrich F, Maazallahi H, Forstmaier A, Winkler D, Hofmann M E G, Denier van der Gon H and Röckmann T 2020 Methane emissions from the Munich Oktoberfest *Atmos. Chem. Phys.* **20** 3683–96

Chen J, Viatte C, Hedelius J K, Jones T, Franklin J E, Parker H, Gottlieb E W, Wennberg P O, Dubey M K and Wofsy S C 2016 Differential column measurements using compact solar-tracking spectrometers *Atmos. Chem. Phys.* **16** 8479–98

Copernicus Climate Change Service (C3S) 2017 ERA5: fifth generation of ECMWF atmospheric reanalyses of the global climate. Copernicus climate change service climate data store (CDS) (https://cds.climate.copernicus.eu/cdsapp#!/home) (Accessed: 5 January 2020)

Crippa M, Solazzo E, Huang G, Guizzardi D, Koffi E, Muntean M, Schieberle C, Friedrich R and Janssens-Maenhout G 2020 High resolution temporal profiles in the Emissions Database for Global Atmospheric Research *Sci. Data* **7** 121

Crisp D 2015 Measuring atmospheric carbon dioxide from space with the orbiting carbon observatory-2 (OCO-2) *Earth Observing Systems XX*

Crisp D *et al* 2012 The ACOS CO_2 retrieval algorithm-part II: global X CO_2 data characterization *Atmos. Meas. Tech.* **5** 687–707

Crisp D *et al* 2017 The on-orbit performance of the orbiting carbon observatory-2 (OCO-2) instrument and its radiometrically calibrated products *Atmos. Meas. Tech.* **10** 59–81

de Gouw J A, Parrish D D, Frost G J and Trainer M 2014 Reduced emissions of CO_2, NO_x, and SO_2 from U.S. power plants owing to switch from coal to natural gas with combined cycle technology *Earths Future* **2** 75–82

EAS (Economic Affairs Sector) 2014 *Agricultural Census for the Agricultural Year 2009–2010—The Total Republic* (Eqypt: Ministry of Agricultural and Land Reclamation)

El Gamal T and Zaki N 2017 Egyptian irrigation after the Aswan high dam *Irrigated Agriculture in Egypt* (Berlin: Springer International Publishing) pp 47–79

El-Beheiry M, Ahmed D, Ammar E and Shaltout K 2015 Diversity of crop plants in Nile Delta, Egypt *Taeckholmia* **35** 77–97

El-Gafy I K E-D and El-Bably W F 2016 Assessing greenhouse gasses emitted from on-farm irrigation pumps: case studies from Egypt *Ain Shams Eng. J.* **7** 939–51

Fasoli B, Lin J C, Bowling D R, Mitchell L and Mendoza D 2018 Simulating atmospheric tracer concentrations for spatially distributed receptors: updates to the stochastic time-inverted Lagrangian transport model's R interface (STILT-R version 2) *Geosci. Model Dev.* **11** 2813–24

Food and Agriculture Organization of the United Nations 2019 FAOSTAT Database (www.fao.org/faostat/en/#data/QC) (Accessed: 11 November 2019)

Frankenberg C *et al* 2011 New global observations of the terrestrial carbon cycle from GOSAT: patterns of plant fluorescence with gross primary productivity *Geophys. Res. Lett.* **38** 17

Frankenberg C, O'Dell C, Berry J, Guanter L, Joiner J, Köhler P, Pollock R and Taylor T E 2014 Prospects for chlorophyll fluorescence remote sensing from the orbiting carbon observatory-2 *Remote Sens. Environ.* **147** 1–12

Frankenberg C *et al* 2015 The orbiting carbon observatory (OCO-2): spectrometer performance evaluation using pre-launch direct sun measurements *Atmos. Meas. Tech.* **8** 301–13

Gately C K and Hutyra L R 2017 Large uncertainties in urban-scale carbon emissions *J. Geophys. Res. Atmos.* **122** 11,242–11,260

Gerbig C, Lin J C, Wofsy S C, Daube B C, Andrews A E, Stephens B B, Bakwin P S and Grainger C A 2003 Toward constraining regional-scale fluxes of CO 2 with atmospheric observations over a continent: 2. Analysis of COBRA data using a receptor-oriented framework *J. Geophys. Res. Atmos.* **108** 4757

Guan D, Liu Z, Geng Y, Lindner S and Hubacek K 2012 The gigatonne gap in China's carbon dioxide inventories *Nat. Clim. Chang.* **2** 672–5

Hakkarainen J, Ialongo I, Maksyutov S and Crisp D 2019 Analysis of four years of global XCO2 anomalies as seen by orbiting carbon observatory-2 *Remote Sens.* **11** 850

Hakkarainen J, Ialongo I and Tamminen J 2016 Direct space-based observations of anthropogenic CO 2 emission areas from OCO-2 *Geophys. Res. Lett.* **43** 11,400–11,406

Hannam K D, Midwood A J, Neilsen D, Forge T A and Jones M D 2019 Bicarbonates dissolved in irrigation water contribute to soil CO 2 efflux *Geoderma* **337** 1097–104

Hollmann R *et al* 2013 The ESA climate change initiative: satellite data records for essential climate Variables *Bull. Am. Meteorol. Soc.* **94** 1541–52

Hu C, Griffis T J, Lee X, Millet D B, Chen Z, Baker J M and Xiao K 2018a Top-down constraints on anthropogenic CO 2 emissions within an agricultural-urban landscape *J. Geophys. Res. Atmos.* **123** 4674–94

Hu C, Liu S, Wang Y, Zhang M, Xiao W, Wang W and Xu J 2018b Anthropogenic CO 2 emissions from a megacity in the Yangtze River Delta of China *Environ. Sci. Pollut. Res.* **25** 23157–69

Hutyra L R, Duren R, Gurney K R, Grimm N, Kort E A, Larson E and Shrestha G 2014 Urbanization and the carbon cycle: current capabilities and research outlook from the natural sciences perspective *Earths Future* **2** 473–95

IPCC: Climate Change 2013 *The Physical Science Basis. Contribution of Working Group I to the Fifth Assessment Report of the Intergovernmental Panel on Climate Change*, ed T F Stocker, D Qin, G-K Plattner, M Tignor, S K Allen, J Boschung, A Nauels, Y Xia, V Bex and P M Midgley (Cambridge: Cambridge University Press) (https://www.ipcc.ch/report/ar5/wg1/)

Jacoby W G 2000 Loess: a nonparametric, graphical tool for depicting relationships between variables *Elect. Stud.* **19** 577–613

Janardanan R, Maksyutov S, Oda T, Saito M, Kaiser J W, Ganshin A, Stohl A, Matsunaga T, Yoshida Y and Yokota T 2016 Comparing GOSAT observations of localized CO 2 enhancements by large emitters with inventory-based estimates *Geophys. Res. Lett.* **43** 3486–93

Janssens-Maenhout G *et al* 2019 EDGAR v4.3.2 Global Atlas of the three major greenhouse gas emissions for the period 1970–2012 *Earth Syst. Sci. Data* 11 959–1002

Kort E A, Frankenberg C, Miller C E and Oda T 2012 Space-based observations of megacity carbon dioxide *Geophys. Res. Lett.* **39**

Kuze A *et al* 2016 Update on GOSAT TANSO-FTS performance, operations, and data products after more than 6 years in space *Atmos. Meas. Tech.* **9** 2445–61

Labzovskii L D, Jeong S-J and Parazoo N C 2019 Working towards confident spaceborne monitoring of carbon emissions from cities using orbiting carbon observatory-2 *Remote Sens. Environ.* **233** 111359

Lin J C, Gerbig C, Wofsy S C, Andrews A E, Daube B C, Davis K J and Grainger C A 2003 A near-field tool for simulating the upstream influence of atmospheric observations: the Stochastic Time-Inverted Lagrangian Transport (STILT) model *J. Geophys. Res. Atmos.* **108** 4493

Lindenmaier R, Dubey M K, Henderson B G, Butterfield Z T, Herman J R, Rahn T and Lee S H 2014 Multiscale observations of CO_2, $^{13}CO_2$, and pollutants at four corners for emission verification and attribution *Proc. Natl Acad. Sci. USA* **111** 8386–91

Liu Z *et al* 2015 Reduced carbon emission estimates from fossil fuel combustion and cement production in China *Nature* **524** 335–8

Luther A *et al* 2019 Quantifying CH 4 emissions from hard coal mines using mobile sun-viewing fourier transform spectrometry *Atmos. Meas. Tech.* **12** 5217–30

Mckain K, Wofsy S C, Nehrkorn T, Eluszkiewicz J, Ehleringer J R and Stephens B B 2012 Assessment of ground-based atmospheric observations for verification of greenhouse gas emissions from an urban region *Proc. Natl Acad. Sci.* **109** 8423–8

Miller S M *et al* 2013 Anthropogenic emissions of methane in the United States *Proc. Natl Acad. Sci.* **110** 20018–22

Nassar R, Hill T G, McLinden C A, Wunch D, Jones D B A and Crisp D 2017 Quantifying CO 2 emissions from individual power plants from space *Geophys. Res. Lett.* **44** 10045–53

Negm A M, Saavedra O and El-Adawy A 2016 *Nile Delta Biography: Challenges and Opportunities Handbook of Environmental Chemistry* (Berlin: Springer) pp 3–18

O'Dell C W *et al* 2012 The ACOS CO 2 retrieval algorithm—part 1: description and validation against synthetic observations *Atmos. Meas. Tech.* **5** 99–121

O'Dell C W *et al* 2018 Improved retrievals of carbon dioxide from orbiting carbon observatory-2 with the version 8 ACOS algorithm *Atmos. Meas. Tech.* **11** 6539–76

Oda T and Maksyutov S 2011 A very high-resolution (1 km × 1 km) global fossil fuel CO 2 emission inventory derived using a point source database and satellite observations of nighttime lights *Atmos. Chem. Phys.* **11** 543–56

Oda T, Maksyutov S and Andres R J 2018 The open-source data inventory for anthropogenic CO₂, version 2016 (ODIAC2016): A global monthly fossil fuel CO₂ gridded emissions data product for tracer transport simulations and surface flux inversions *Earth Syst. Sci. Data* **10** 87–107

Osama S, Elkholy M and Kansoh R M 2017 Optimization of the cropping pattern in Egypt *Alex. Eng. J.* **56** 557–66

Peng J, Tian L, Liu Y, Zhao M, Hu Y and Wu J 2017 Ecosystem services response to urbanization in metropolitan areas: thresholds identification *Sci. Total Environ.* **607–608** 706–14

Peylin P *et al* 2013 Global atmospheric carbon budget: results from an ensemble of atmospheric CO 2 inversions *Biogeosciences* **10** 6699–720

Quéré C *et al* 2018 Global carbon budget 2018 *Earth Syst. Sci. Data* **10** 2141–94

Radwan T M, Blackburn G A, Whyatt J D and Atkinson P M 2019 Dramatic loss of agricultural land due to urban expansion threatens food security in the Nile Delta, Egypt *Remote Sens.* **11** 1–20

Rana G, Ferrara R M, Vitale D, D'Andrea L and Palumbo A D 2016 Carbon assimilation and water use efficiency of a

perennial bioenergy crop (cynara cardunculus L.) in mediterranean environment *Agric. For. Meteorol.* **217** 137–50

Reuter M, Buchwitz M, Schneising O, Krautwurst S, O'Dell C W, Richter A, Bovensmann H and Burrows J P 2019 Towards monitoring localized CO_2 emissions from space: co-located regional CO_2 and NO_2 enhancements observed by the OCO-2 and S5P satellites *Atmos. Chem. Phys.* **19** 9371–83

Schneising O, Heymann J, Buchwitz M, Reuter M, Bovensmann H and Burrows J P 2013 Anthropogenic carbon dioxide source areas observed from space: assessment of regional enhancements and trends *Atmos. Chem. Phys.* **13** 2445–54

Schwandner F M *et al* 2017 Spaceborne detection of localized carbon dioxide sources *Science* **358** eaam5782

She W, Wu Y, Huang H, Chen Z, Cui G, Zheng H, Guan C and Chen F 2017 Integrative analysis of carbon structure and carbon sink function for major crop production in China's typical agriculture regions *J. Clean. Prod.* **162** 702–8

Shekhar A, Bhattacharjee S, Chen J and Rammig A 2019 Spring-summer variation analysis in OCO-2's solar induced fluorescence during the European heatwave in 2018 *Geophys. Res. Abstr.* **21** EGU2019-17409-1

Sun Y *et al* 2017 OCO-2 advances photosynthesis observation from space via solar-induced chlorophyll fluorescence *Science* **358** eaam5747

Telmer K and Veizer J 1999 Carbon fluxes, pCO2 and substrate weathering in a large northern river basin, Canada: carbon isotope perspectives *Chem. Geol.* **159** 61–86

Viatte C *et al* 2017 Methane emissions from dairies in the Los Angeles Basin *Atmos. Chem. Phys.* **17** 7509–28

Wang R *et al* 2013 High-resolution mapping of combustion processes and implications for CO_2 emissions *Atmos. Chem. Phys.* **13** 5189–203

Wang S, Zhang Y, Hakkarainen J, Ju W, Liu Y, Jiang F and He W 2018 Distinguishing anthropogenic CO_2 emissions from different energy intensive industrial sources using OCO-2 observations: a case study in Northern China *J. Geophys. Res. Atmos.* **123** 9462–73

Wu D, Lin J C, Fasoli B, Oda T, Ye X, Lauvaux T, Yang E G and Kort E A 2018 A Lagrangian approach towards extracting signals of urban CO_2 emissions from satellite observations of atmospheric column CO 2 (XCO 2): X-stochastic time-inverted lagrangian transport model ('X-STILT v1') *Geosci. Model Dev.* **11** 4843–71

Wunch D, Toon G C, Blavier J-F L, Washenfelder R A, Notholt J, Connor B J, Griffith D W T, Sherlock V and Wennberg P O 2011a The total carbon column observing network *Philos. Trans. R. Soc.* A **369** 2087–112

Wunch D *et al* 2011b A method for evaluating bias in global measurements of CO_2 total columns from space *Atmos. Chem. Phys.* **11** 12317–37

Xu Q, Dong Y and Yang R 2018 Urbanization impact on carbon emissions in the Pearl River Delta region: kuznets curve relationships *J. Clean. Prod.* **180** 514–23

Xue B and Ren W 2012 China's uncertain CO2 emissions *Nat. Clim. Chang.* **2** 762–762

Ye X, Lauvaux T, Kort E A, Oda T, Feng S, Lin J C, Yang E and Wu D 2017 Constraining fossil fuel CO_2 emissions from urban area using OCO-2 observations of total column CO_2 *Atmos. Chem. Phys. Discuss.* 1–30

Yokota T, Yoshida Y, Eguchi N, Ota Y, Tanaka T, Watanabe H and Maksyutov S 2009 Global concentrations of CO2 and CH4 retrieved from GOSAT: first preliminary results *SOLA* **5** 160–3

Zeydan B A 2005 The nile delta in a global vision *Ninth Int. Water Technol. Conf. IWTC9 2005, Sharm El-Sheikh, Egypt* vol 31 pp 31–40

Zheng T, Nassar R and Baxter M 2019 Estimating power plant CO_2 emission using OCO-2 XCO_2 and high resolution WRF-Chem simulations *Environ. Res. Lett.* **14** 085001

Zhou C, Wang S and Wang J 2019 Examining the influences of urbanization on carbon dioxide emissions in the Yangtze River Delta, China: kuznets curve relationship *Sci. Total Environ.* **675** 472–82